

Phase diagram of the $\text{PrFeAsO}_{1-x}\text{F}_x$ superconductor

C. R. Rotundu,¹ D. T. Keane,² B. Freelon,³ S. D. Wilson,¹ A. Kim,³ P. N. Valdivia,⁴ E. Bourret-Courchesne,⁵ and R. J. Birgeneau^{1,3,4}

¹*Materials Sciences Division, Lawrence Berkeley National Laboratory, Berkeley, California 94720, USA*

²*DND-CAT, Advanced Photon Source, Argonne National Laboratory, Argonne, Illinois 60439, USA*

³*Department of Physics, University of California, Berkeley, California 94720, USA*

⁴*Department of Materials Science and Engineering, University of California, Berkeley, California 94720, USA*

⁵*Life Sciences Division, Lawrence Berkeley National Laboratory, Berkeley, California 94720, USA*

(Received 7 July 2009; revised manuscript received 23 September 2009; published 15 October 2009)

The electronic phase diagram of $\text{PrFeAsO}_{1-x}\text{F}_x$ ($0 \leq x \leq 0.225$) has been determined using synchrotron x-ray powder-diffraction, magnetization, and resistivity measurements. The structural transition temperature is suppressed from 154 to ≈ 120 K and the magnetic phase transitions of both iron and praseodymium ions are completely suppressed by $x \approx 0.08$ fluorine doping, coinciding with the emergence of superconductivity. The optimal doping is $x \approx 0.15$ when $T_C = 47$ K while the maximum solubility of fluorine in $\text{PrFeAsO}_{1-x}\text{F}_x$ is reached around $x = 0.22$. The structural, magnetic, and superconducting phase diagram is presented.

DOI: [10.1103/PhysRevB.80.144517](https://doi.org/10.1103/PhysRevB.80.144517)

PACS number(s): 74.25.Dw, 74.25.Fy, 74.25.Ha, 74.70.-b

I. INTRODUCTION

The discovery of superconductivity in the oxypnictides LnMPnO ($\text{Ln} = \text{La-Nd, Sm, and Gd}$; $\text{M} = \text{Fe, Co, Ni, and Ru}$; $\text{Pn} = \text{P and As}$)¹⁻⁴ with a ZrCuSiAs -type structure^{5,6} sets a milestone in the field of superconductivity. The first step in the study of a discovered superconductor and toward elucidation of the nature of superconductivity itself is the determination of the phase diagram. It is natural then to compare the pnictide phase diagram with that of the only other class of high-temperature superconductors, the cuprates.⁷⁻¹⁰ As in the cuprates, superconductivity arises when a so-called parent nonsuperconducting compound is doped with charge carriers. It has been demonstrated that the parent compound, LnFeAsO , can be doped with holes when Ln^{3+} is replaced partially by a divalent ion ($\text{La}_{1-x}\text{Sr}_x\text{FeAsO}$,¹¹ $\text{Pr}_{1-x}\text{Sr}_x\text{FeAsO}$,¹² and Sr^{2+}). Correspondingly, n -type doping is realized either by substitution of Ln^{3+} by a tetravalent ion [$\text{Gd}_{1-x}\text{Th}_x\text{FeAsO}$ (Ref. 13) and Th^{4+}] or partially replacing O^{2-} by F^- . Among the iron pnictides, to date, the electron-doped (O_{1-x}F_x) iron arsenides $\text{LnFeAsO}_{1-x}\text{F}_x$ have the highest T_C 's reported. Until now, there have been reports on the phase diagrams of $\text{LnFeAsO}_{1-x}\text{F}_x$, $\text{Ln} = \text{La}$,^{1,10,14-17} Ce ,^{2,7} Nd ,¹⁸ and Sm .¹⁹⁻²¹ Within the phase diagram of $\text{CeFeAsO}_{1-x}\text{F}_x$, Zhao *et al.*⁷ argue for a suppression of the antiferromagnetism (AFM) with doping such that the magnetic order vanishes in the close proximity to the superconductivity (SC). This has been confirmed in other $\text{LnFeAsO}_{1-x}\text{F}_x$ systems.^{2,7,10,14-19} Yet, in $\text{SmFeAsO}_{1-x}\text{F}_x$ there are reports of coexistence of static AFM order with superconductivity.^{20,21} Also, a signature of the Sm^{3+} ions' magnetism has been reported in optimal superconducting $\text{SmFeAsO}_{0.85}\text{F}_{0.15}$.²² More recent studies on homolog systems^{10,15,16} report a rather *abrupt* (first-orderlike) change in the structural and magnetic-order parameters at the boundary of superconductivity. Despite wide efforts toward a unified picture, a consensus has not yet been reached. Without any doubt, the correctness of the phase diagrams relies on an accurate determination of the fluorine-ion concentration.^{10,23}

In this paper, we use synchrotron x-ray scattering, magnetization, and resistivity measurements to map the structural, magnetic, and superconducting phase diagram of the less studied $\text{PrFeAsO}_{1-x}\text{F}_x$.

II. EXPERIMENTAL PROCEDURE

$\text{PrFeAsO}_{1-x}\text{F}_x$ polycrystalline samples were synthesized through a two-step standard high-temperature solid-state chemical reaction using stoichiometric amounts of PrAs , Fe (4N8), Fe_2O_3 (5N), and PrF_3 (4N) as starting materials.^{3,19} The PrAs binary used in the final reaction was synthesized by reacting Pr (3N) and As (4N) powders. The $\text{Pr}:\text{As} = 1:1$ mix was encapsulated within a tantalum tube that was sealed inside a quartz tube under a low-pressure Ar atmosphere, slowly heated to 500°C , and held at that temperature for 5 h. The powder was ground, mixed, resealed, and heated again to 900°C for 10 h. The stoichiometric constituents were then thoroughly ground, mixed, and finally pressed into pellets using a cold isostatic press with a pressure of 0.38 GPa. To avoid direct contact with the quartz tube and possible Si contamination, the pellets were wrapped in tantalum foil before being sealed under a low atmosphere of Ar gas in quartz tubes. They were heated to 1150°C for 50 h. All preparatory steps except the annealing were performed in a glovebox under a high-purity Ar-gas atmosphere. The single phase was checked after each step using x-ray diffraction (XRD) with $\text{Cu } K\alpha$ radiation at room temperature. A discrepancy between the nominal and real fluorine content has been systematically reported in homolog systems.^{10,23} Therefore we determined the actual fluorine concentration by wavelength-dispersive x-ray spectroscopy (WDS) for each concentration. Therefore, all fluorine concentrations reported in this paper are the as-measured values and not the nominal starting compositions. Figure 1 shows the actual fluorine-doping x (WDS) as measured by WDS versus the initial (nominal) concentration. As pointed by Ref. 23, the actual doping of the primary phase is less than nominal (Fig. 1) because of fluorine incorporation in secondary phases, for-

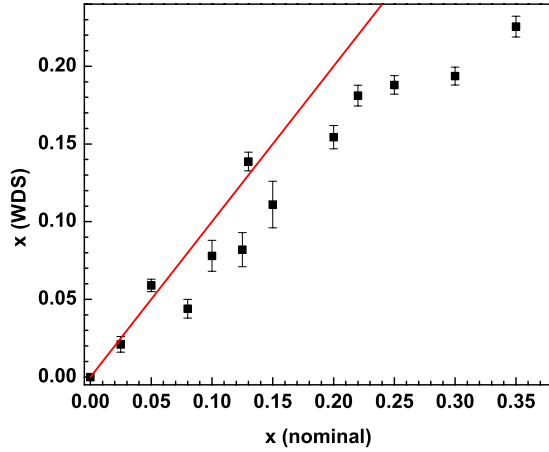


FIG. 1. (Color online) The actual fluorine concentration $x(\text{WDS})$ as measured by WDS versus the nominal concentration $x(\text{nominal})$. The solid line it is a guide for the eyes of $x(\text{WDS}) = x(\text{nominal})$.

mation of volatile components and absorption from the tantalum wrapping foil and quartz tube. Resistivity, dc- and ac-susceptibility measurements down to 1.8 K were performed using a Quantum Design physical property measurements system. Electrical contacts with the samples for resistivity measurements were made using Pelco colloidal silver paste through attaching thin gold wires in a four-probe configuration.

The silver paste was cured at 100 °C for up to 30 min in order to avoid sample degradation. The excitation current of 2 mA was optimized for the best signal-to-noise ratio and to prevent overheating of the samples by checking the linear I - V characteristics. Because the absolute values of the resistivity data carry an uncertainty of up to 30% due to the slightly off-rectangular shape of the bar-shaped samples and the size of the contact pads, we report instead resistivity data as normalized to the room-temperature values. The ac susceptibility was measured with a 10 Oe modulated field of frequency $f=1$ kHz while dc measurements were carried out in 200 Oe. Synchrotron x-ray powder-diffraction measurements with an incident-beam wavelength $\lambda=0.31$ Å were performed at DND-CAT, Advanced Photon Source, Argonne National Laboratory.

III. RESULTS AND DISCUSSION

The parent PrFeAsO antiferromagnetic semimetal crystallizes in a $P4/nmm$ tetragonal structure at high temperatures but undergoes a ($Cmma$) orthorhombic transformation at low temperatures,²⁴ which is characteristic of all $Ln\text{FeAsO}$ systems. In order to obtain insight into the evolution of the crystallographic structure with fluorine doping and its relevance for superconductivity, we performed synchrotron x-ray powder-diffraction measurements on the undoped parent PrFeAsO , two nonsuperconducting samples $x=0.059$ and 0.078 , and one underdoped superconducting concentration with $x=0.082$.

Figure 2 shows 2θ scans through the $(2\ 2\ 0)_T$ Bragg

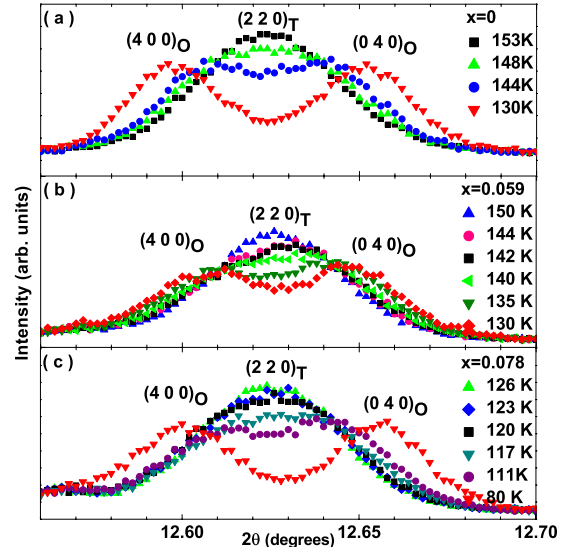


FIG. 2. (Color online) The profile of the $(2\ 2\ 0)_T$ XRD peak of the $P4/nmm$ tetragonal structure splitting below T_S into the $(4\ 0\ 0)_O$ and $(0\ 4\ 0)_O$ reflections of the $Cmma$ orthorhombic phase of nonsuperconducting $\text{PrFeAsO}_{1-x}\text{F}_x$ (a) $x=0$, $T_S=154$ K, (b) $x=0.059$, $T_S=142$ K, and (c) $x=0.078$, $T_S=120$ K. T and O subscripts denote tetragonal and orthorhombic, respectively.

peak of the high-temperature $P4/nmm$ tetragonal structure. The peak broadens and splits into the $(4\ 0\ 0)_O$ and $(0\ 4\ 0)_O$ peaks of the $Cmma$ orthorhombic phase upon cooling. “T” and “O” subscripts denote tetragonal and orthorhombic, respectively. The corresponding structural transition temperatures found within ± 2 K resolution are $T_S=154$ K for the parent, $T_S=142$ K for $x=0.059$, and $T_S=120$ K for the fluorine doping preceding superconductivity $x=0.078$.

Figure 3 shows the evolution of the $(2\ 2\ 0)$ Bragg peak for the superconducting $x=0.082$ sample upon cooling to 50 K. The full width at half maximum (FWHM) of the peak is plotted versus temperature in the inset of Fig. 3 and shows a continuous evolution down to 50 K. Upon cooling, we observe a continuous slight broadening of the $(2\ 2\ 0)$ peak; yet

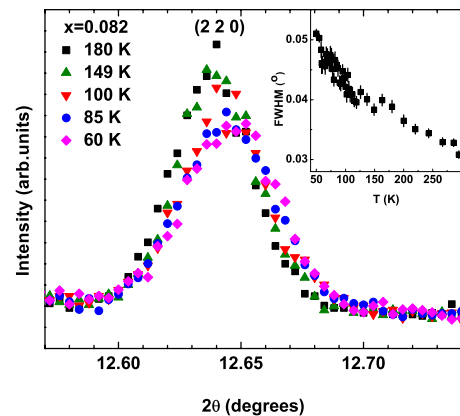


FIG. 3. (Color online) The profile of the $(2\ 2\ 0)$ XRD peak of the tetragonal superconducting $\text{PrFeAsO}_{1-x}\text{F}_x$, $x=0.082$. The inset shows the FWHM of the peak versus temperature.

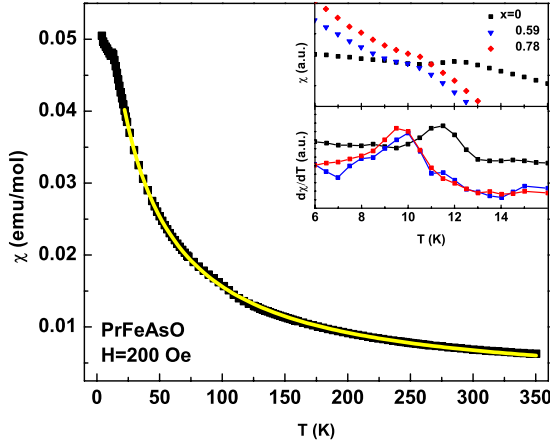


FIG. 4. (Color online) The temperature-dependent magnetic susceptibility of PrFeAsO . The yellow (or light gray) curve is the result of a fit to Curie-Weiss law. The upper inset shows the susceptibility of $\text{PrFeAsO}_{1-x}\text{F}_x$, with $x=0, 0.059$, and 0.078 around the Pr-ion ordering temperature along with their derivatives in the lower inset. In the lower panel the line is a guide to the eyes.

we were not able to resolve any definite inflection point in the FWHM versus T indicative of a signature of the tetragonal to orthorhombic structural phase transition.⁷ Therefore, our data support a picture of a rather abrupt suppression of the orthorhombic phase at the boundary of superconductivity. Our best estimate is a complete suppression of T_S from 120 K within 2.5% fluorine doping of the critical value for superconductivity (x between 0.068 and 0.093).

Now we turn to our magnetic-susceptibility data. Figure 4 shows the temperature-dependent dc magnetic susceptibility of PrFeAsO measured in 200 Oe fitted above the Pr ordering temperature with a Curie-Weiss law, $\chi(T) = \chi_0 + C/(T + \theta)$, where χ_0 is the temperature-independent susceptibility, $C = N\mu_{\text{eff}}^2/3k_B$ is the Curie constant, N is the number of Pr^{3+} ions, and θ is the Curie-Weiss temperature. The effective moment found is $\mu_{\text{eff}} = 3.75\mu_B$, slightly larger than the isolated trivalent Pr-ion value of $3.58\mu_B$.²⁵ The discrepancy could be due to the Pr^{3+} crystalline electric field contribution to the susceptibility.²⁶ It should be noted that the susceptibility data could be fitted with a Curie-Weiss law for $\text{LnFeAsO}_{1-x}\text{F}_x$, $\text{Ln} = \text{Ce},^{2,27} \text{Nd},^{27}$ and Gd (Ref. 13) but not in the case of $\text{Ln} = \text{Sm}$.²⁸ The low-temperature susceptibility is dominated by a sharp peak around 12 K in the pure PrFeAsO system, as well as in all other nonsuperconducting F^- concentrations. This is due to the AFM ordering (Néel temperature) of the Pr $4f$ electrons [Fig. 6(b)], consistent with previous reports from neutron,²⁴ magnetization,²⁷ and resistivity^{27,29} studies. The upper inset shows a moderated suppression of $T_N(\text{Pr})$ with fluorine doping for three different concentrations $x=0, 0.059$, and 0.078 in $\text{PrFeAsO}_{1-x}\text{F}_x$ extending over the whole nonsuperconducting region. In the lower inset the temperature derivative of the susceptibility around the ordering temperature is shown. Again, it should be noted that there is a weak to moderate suppression of the ordering temperature with fluorine doping.

Figure 5 presents the real components of the ac susceptibilities normalized to their corresponding maxima for the

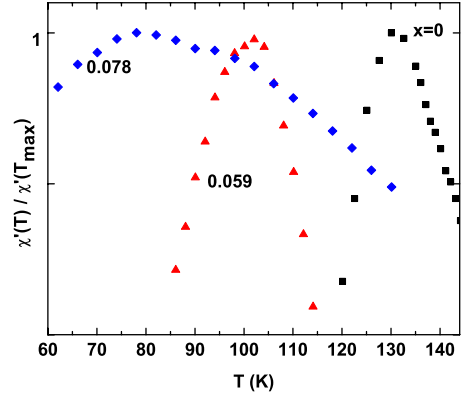


FIG. 5. (Color online) Real component of ac susceptibility normalized to its maximum of $\text{PrFeAsO}_{1-x}\text{F}_x$, with $x=0, 0.059$, and 0.078 .

same compositions ($x=0, 0.059, 0.78$) discussed previously. The 130 K sharp peak in magnetization of the parent compound coincides with the magnetic-ordering temperature of the iron-ion moments, as initially revealed by the neutron-diffraction data.²⁴ With fluorine doping, the magnetic-ordering temperature of the iron moments is continuously reduced from 130 ($x=0$) to 80 K for $x=0.078$.

In Fig. 6 we show resistivity data for $\text{PrFeAsO}_{1-x}\text{F}_x$ with $x=0, 0.044, 0.11, 0.138$, and 0.225 divided by the room-temperature value, $\rho(297 \text{ K})$. The data are shifted for clarity. The behavior of $\rho(T)$ for the PrFeAsO compound is similar to that of the other LnFeAsO , $\text{Ln} = \text{La}, \text{Ce}, \text{Nd}$, and Sm .^{19,27} Upon cooling, the resistivity decreases showing metallic behavior. Around 150 K there is a broad peak associated with both the structural phase transition from tetragonal to orthorhombic symmetry and the spin-density-wave magnetic

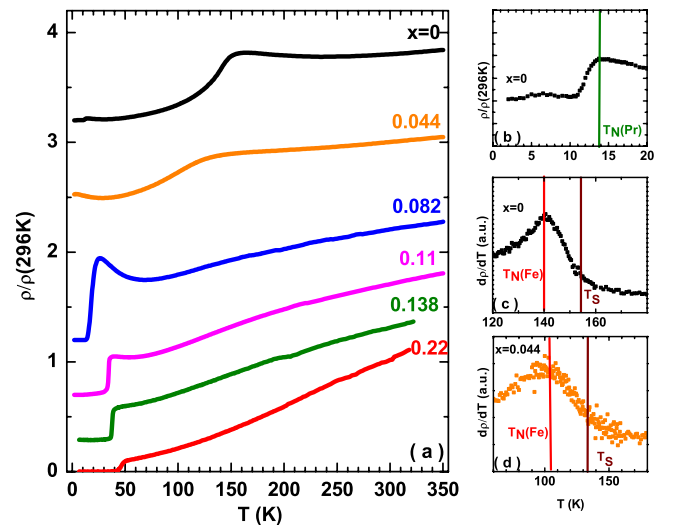


FIG. 6. (Color online) (a) Resistivity of $\text{PrFeAsO}_{1-x}\text{F}_x$ for $x=0, 0.044, 0.11, 0.138$, and 0.225 divided by the room-temperature value. Data is shifted for clarity. (b) The resistivity near the Pr-ion ordering temperature [$T_N(\text{Pr})$] for the parent PrFeAsO . The temperature derivative of the resistivity ($\partial\rho/\partial T$) for (c) $x=0$ and (d) $x=0.044$. T_S and T_N mark the structural and the magnetic phase transitions, respectively.

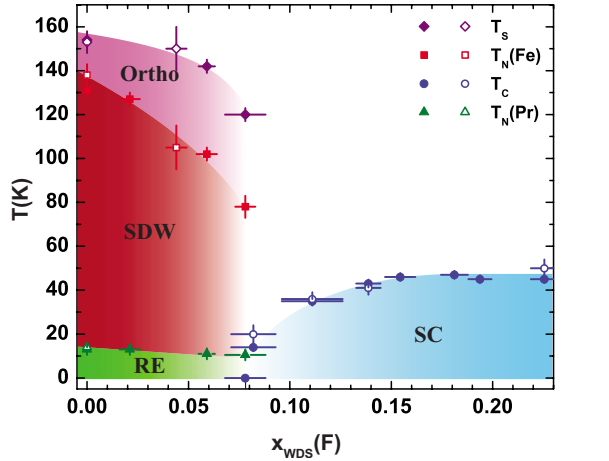


FIG. 7. (Color online) The structural, magnetic, and superconducting phase diagram of $\text{PrFeAsO}_{1-x}\text{F}_x$, $0 \leq x \leq 0.225$ as determined from our synchrotron x-ray powder-diffraction, magnetization, and resistivity measurements. The $P4/nmm$ to $Cmma$ phase transition as determined from x-ray powder diffraction (\blacklozenge) and from the temperature derivative of the resistivity $\partial\rho/\partial T$ (\diamond). The Néel temperatures of Fe [$T_N(\text{Fe})$] and Pr [$T_N(\text{Pr})$] ions as determined from magnetization (\blacksquare , \blacktriangle) and from ρ or $\partial\rho/\partial T$ (\square , \triangle), respectively. The superconducting transition temperatures T_C for samples with fluorine doping between ~ 0.08 and 0.225 were determined from susceptibility (\bullet) and from the drop of the resistivity (\circ).

phase transition. Because of a smooth and continuous change in the physical properties around these transitions, an indicator of the transition temperature is the temperature derivative of the resistivity.^{10,16,27,30} Figures 6(c) and 6(d) show $\partial\rho/\partial T$ for the $x=0$ and 0.044 nonsuperconducting samples. $T_N(\text{Fe})$ and T_S correspond to the two inflection points in $\partial\rho/\partial T$. At around 13 K, the resistivity of the parent PrFeAsO exhibits a shoulderlike feature [Fig. 6(b)] that was attributed to the AFM ordering of the Pr-ion moments.^{27,29}

Figure 7 shows the phase diagram of $\text{PrFeAsO}_{1-x}\text{F}_x$ ($0 \leq x \leq 0.225$) as determined by the measurements reported in this paper. Superconductivity appears after doping with charge carriers (electrons) the parent AFM semimetal PrFeAsO . In this system, doping is realized by substituting O^{2-} by F^- . Upon doping, the coupled structural and AFM transitions are suppressed, in analogy with the behavior of the structural and magnetic transitions in $\text{La}_{2-x}\text{Sr}_x\text{CuO}_4$.³¹ The phase diagram showing close proximity between AFM and SC resembles that of the electron-doped cuprates where the AFM persists right up to the SC dome. The superconducting transition temperatures were determined by the onset of the diamagnetism in zero-field-cooled magnetization (data not shown) or the drop of the resistivity. Optimal doping is achieved at a fluorine concentration of ≈ 0.15 , in agreement with values reported for the homologous systems $\text{CeFeAsO}_{1-x}\text{F}_x$ (Refs. 2 and 7) and $\text{SmFeAsO}_{1-x}\text{F}_x$ (Refs. 3, 19, and 21) and as predicted by recent minimum principle-energy calculations.³² $\text{LnFeAsO}_{1-\delta}$ oxygen deficient (optimally doped at $\delta=0.15$) with no fluorine doping obtained by high-pressure synthesis has been reported to be a superconductor;³³ this process is similar to the well-known

oxygenation of the cuprates. It is worthwhile to mention that a maximum superconducting temperature transition around 47 K has been reported previously for optimally doped samples synthesized by normal pressure solid-state chemical reaction^{29,34} while a slightly enhanced T_C of 52 K was reported for the samples synthesized using a high-pressure method.⁴ Our results show that the synthesis of a sample with nominal fluorine concentration of 0.35 resulted in an actual fluorine x_{WDS} substitution of 0.225, which represents the maximum fluorine doping in $\text{PrFeAsO}_{1-x}\text{F}_x$. This value is consistent with recently reported WDS determined values in $\text{LaFeAsO}_{1-x}\text{F}_x$ and $\text{SmFeAsO}_{1-x}\text{F}_x$ (Ref. 23) and the saturation of lattice parameters in $\text{LaFeAsO}_{1-x}\text{F}_x$.³⁵

IV. CONCLUSIONS

In summary, we have determined the complete structural, magnetic, and superconducting phase diagram of $\text{PrFeAsO}_{1-x}\text{F}_x$ ($0 \leq x \leq 0.22$) using synchrotron x-ray powder-diffraction, magnetization, and resistivity measurements. We find a progressive suppression of the structural transition and magnetic-ordering transitions of both iron- and praseodymium-ion moments with increasing fluorine doping. In superconducting samples, near the edge of the emergence of the superconductivity ($x \approx 0.08$ fluorine doping), we were not able to detect any fraction of the orthogonal phase. The optimal doping was found to be at $x \sim 0.15$ when $T_C = 47$ K, and the maximum fluorine doping in $\text{PrFeAsO}_{1-x}\text{F}_x$ was reached around $x = 0.22$ with superconductivity remaining robust.

The phase diagram is most similar to that of the hole-doped cuprates $\text{La}_{2-x}\text{Sr}_x\text{CuO}_4$.³¹ However, there are some important differences. First, in $\text{La}_{2-x}\text{Sr}_x\text{CuO}_4$ there is a spin-glass phase in between the three-dimensional Néel antiferromagnet and the superconductor; the stripelike spin fluctuations in the cuprate spin-glass phase are rotated by 45° , relative to those in the superconductor and the spin-glass superconductor transition at 0 K as a function of hole concentration is first order. Second, the tetragonal-orthorhombic structural transition temperature in $\text{La}_{2-x}\text{Sr}_x\text{CuO}_4$ varies smoothly across the insulating to superconductor boundary and, indeed, persists in x beyond the value at which T_C is a maximum. By contrast, in the $\text{PrFeAsO}_{1-x}\text{F}_x$ system both the Néel order and the tetragonal-orthorhombic structural transition appear to vanish together quite rapidly, possibly in a first-order way, as the fluorine concentration is varied through the critical value for superconductivity. In order to elucidate this further it will be necessary to prepare homogeneous samples in which the fluorine concentration, x , is varied in quite fine steps. This will represent a significant technical challenge. It will also be necessary to characterize the magnetism in samples in the transition region using both neutron scattering and a local technique such as muon-spin resonance. Of course, the ultimate goal is to determine which features are universal and which are details of a particular system. Specifically, one would like to determine whether or not the iron pnictides and the cuprates are in the same universality class or whether, in fact, the similarity in the phase diagrams is coincidental.

ACKNOWLEDGMENTS

The authors thank S. M. Hanrahan, C. Ramsey, K. Ross, and J. Wu for technical support. This work was supported by the Director, Office of Science, Office of Basic Energy Sciences, U.S. Department of Energy under Contract No. DE-AC02-05CH11231 and Office of Basic Energy Sciences, U.S. DOE under Grant No. DE-AC03-76SF008. Work at Ad-

vanced Photon Source (APS) was performed at the DuPont-Northwestern-Dow Collaborative Access Team (DND-CAT) located at Sector 5 APS. DND-CAT is supported by E.I. DuPont de Nemours & Co., The Dow Chemical Co., and the State of Illinois. Use of the APS was supported by the U. S. Department of Energy, Office of Science, Office of Basic Energy Sciences, under Contract No. DE-AC02-06CH11357.

- ¹Y. Kamihara, T. Watanabe, M. Hirano, and H. Hosono, *J. Am. Chem. Soc.* **130**, 3296 (2008).
- ²G. F. Chen, Z. Li, D. Wu, G. Li, W. Z. Hu, J. Dong, P. Zheng, J. L. Luo, and N. L. Wang, *Phys. Rev. Lett.* **100**, 247002 (2008).
- ³X. H. Chen, T. Wu, G. Wu, R. H. Liu, H. Chen, and D. F. Fang, *Nature (London)* **453**, 761 (2008).
- ⁴Z.-A. Ren, J. Yang, W. Lu, W. Yi, G.-C. Che, X.-L. Dong, L.-L. Sun, and Z.-X. Zhao, *Mater Res. Innovations* **12**, 105 (2008).
- ⁵B. I. Zimmer, W. Jeitschko, J. H. Albering, R. Glaum, and M. Reehuis, *J. Alloys Compd.* **229**, 238 (1995).
- ⁶P. Quebe, L. J. Terbüchte, and W. Jeitschko, *J. Alloys Compd.* **302**, 70 (2000).
- ⁷J. Zhao, Q. Huang, C. de la Cruz, S. Li, J. W. Lynn, Y. Chen, M. A. Green, G. F. Chen, G. Li, Z. Li, J. L. Luo, N. L. Wang, and P. Dai, *Nature Mater.* **7**, 953 (2008).
- ⁸S. A. Kivelson and H. Yao, *Nature Mater.* **7**, 927 (2008).
- ⁹Y. Uemura, *Nature Mater.* **8**, 253 (2009).
- ¹⁰C. Hess, A. Kondrat, A. Narduzzo, J. E. Hamann-Borrero, R. Klingeler, J. Werner, G. Behr, and B. Büchner, *EPL* **87**, 17005 (2009).
- ¹¹H.-H. Wen, G. Mu, L. Fang, H. Yang, and X. Zhu, *EPL* **82**, 17009 (2008).
- ¹²G. Mu, B. Zeng, X. Zhu, F. Han, P. Cheng, B. Shen, and H.-H. Wen, *Phys. Rev. B* **79**, 104501 (2009).
- ¹³C. Wang, L. Li, S. Chi, Z. Zhu, Z. Ren, Y. Li, Y. Wang, X. Lin, Y. Luo, S. Jiang, X. Xu, G. Cao, and Z. Xu, *EPL* **83**, 67006 (2008).
- ¹⁴Y. Kohama, Y. Kamihara, M. Hirano, H. Kawaji, T. Atake, and H. Hosono, *Phys. Rev. B* **78**, 020512(R) (2008).
- ¹⁵H. Luetkens, H.-H. Klauss, M. Kraken, F. J. Litterst, T. Dellmann, R. Klingeler, C. Hess, R. Khasanov, A. Amato, C. Baines, M. Kosmala, O. J. Schumann, M. Braden, J. Hamann-Borrero, N. Leps, A. Kondrat, G. Behr, J. Werner, and B. Büchner, *Nature Mater.* **8**, 305 (2009).
- ¹⁶R. Klingeler, N. Leps, I. Hellmann, A. Popa, C. Hess, A. Kondrat, J. Hamann-Borrero, G. Behr, V. Kataev, and B. Büchner, *arXiv:0808.0708* (unpublished).
- ¹⁷Q. Huang, J. Zhao, J. W. Lynn, G. F. Chen, J. L. Luo, N. L. Wang, and P. Dai, *Phys. Rev. B* **78**, 054529 (2008).
- ¹⁸G. F. Chen, Z. Li, D. Wu, J. Dong, G. Li, W. Z. Hu, P. Zheng, J. L. Luo, and N. L. Wang, *Chin. Phys. Lett.* **25**, 2235 (2008).
- ¹⁹R. H. Liu, G. Wu, T. Wu, D. F. Fang, H. Chen, S. Y. Li, K. Liu, Y. L. Xie, X. F. Wang, R. L. Yang, L. Ding, C. He, D. L. Feng, and X. H. Chen, *Phys. Rev. Lett.* **101**, 087001 (2008).
- ²⁰S. Margadonna, Y. Takabayashi, M. T. McDonald, M. Brunelli, G. Wu, R. H. Liu, X. H. Chen, and K. Prassides, *Phys. Rev. B* **79**, 014503 (2009).
- ²¹A. J. Drew, Ch. Niedermayer, P. J. Baker, F. L. Pratt, S. J. Blundell, T. Lancaster, R. H. Liu, G. Wu, X. H. Chen, I. Watanabe, V. K. Malik, A. Dubroka, M. Rössle, K. W. Kim, C. Baines, and C. Bernhard, *Nature Mater.* **8**, 310 (2009).
- ²²L. Ding, C. He, J. K. Dong, T. Wu, R. H. Liu, X. H. Chen, and S. Y. Li, *Phys. Rev. B* **77**, 180510(R) (2008).
- ²³A. Köhler and G. Behr, *J. Supercond. Novel Magn.* **22**, 565 (2009).
- ²⁴J. Zhao, Q. Huang, C. de la Cruz, J. W. Lynn, M. D. Lumsden, Z. A. Ren, J. Yang, X. Shen, X. Dong, Z. Zhao, and P. Dai, *Phys. Rev. B* **78**, 132504 (2008).
- ²⁵N. W. Ashcroft and D. N. Mermin, *Solid State Physics* (Brooks-Cole, Belmont, MA, 1976).
- ²⁶S. D. Wilson, C. R. Rotundu, D. Abernathy, P. N. Valdivia, S. Hanrahan, E. Bourret-Courchesne, and R. J. Birgeneau (unpublished).
- ²⁷M. A. McGuire, R. P. Hermann, A. S. Sefat, B. C. Sales, R. Jin, D. Mandrus, F. Grandjean, and G. J. Long, *New J. Phys.* **11**, 025011 (2009).
- ²⁸A. Martinelli, M. Ferretti, P. Manfrinetti, A. Palenzona, M. Tropeano, M. R. Cimberle, C. Ferdeghini, R. Valle, C. Bernini, M. Putti, and A. S. Siri, *Supercond. Sci. Technol.* **21**, 095017 (2008).
- ²⁹S. A. J. Kimber, D. N. Argyriou, F. Yokaichiya, K. Habicht, S. Gerischer, T. Hansen, T. Chatterji, R. Klingeler, C. Hess, G. Behr, A. Kondrat, and B. Büchner, *Phys. Rev. B* **78**, 140503(R) (2008).
- ³⁰H.-H. Klauss, H. Luetkens, R. Klingeler, C. Hess, F. J. Litterst, M. Kraken, M. M. Korshunov, I. Eremin, S.-L. Drechsler, R. Khasanov, A. Amato, J. Hamann-Borrero, N. Leps, A. Kondrat, G. Behr, J. Werner, and B. Büchner, *Phys. Rev. Lett.* **101**, 077005 (2008).
- ³¹R. J. Birgeneau, C. Stock, J. M. Tranquada, and K. Yamada, *J. Phys. Soc. Jpn.* **75**, 111003 (2006).
- ³²X. Huang, *arXiv:0807.0899* (unpublished).
- ³³Z.-A. Ren, G.-C. Che, X.-L. Dong, J. Yang, W. Lu, W. Yi, X.-L. Shen, Z.-C. Li, L.-L. Sun, F. Zhou, and Z.-X. Zhao, *EPL* **83**, 17002 (2008).
- ³⁴D. Bhoi, P. Mandal, and P. Choudhury, *Supercond. Sci. Technol.* **21**, 125021 (2008).
- ³⁵A. Kondrat, J. E. Hamann-Borrero, N. Leps, M. Kosmala, O. Schumann, J. Werner, G. Behr, M. Braden, R. Klingeler, B. Büchner, and C. Hess, *Eur. Phys. J. B* **70**, 461 (2009).